The neglected influence of zinc oxide light-soaking on stability measurements of inverted organic solar cells

Marcella Günther, Soroush Lotfi, Sergio Sánchez Rivas, Dominic Blätte, Jan P. Hofmann, Thomas Bein, and Tayebeh Ameri*

Although zinc oxide (ZnO) is one of the most commonly used materials for electron transport layers in organic solar cells (OSCs), it also comes with disadvantages such as the so-called light-soaking issues, i.e., its need for exposure to UV light to reach its full potential in OSCs. Here, the impact of ZnO light-soaking issues on stability measurements of OSCs is investigated. It is found that in the absence of UV light a reversible degradation occurs, which is independent of the used active layer material and accelerates at higher temperatures but can be undone with a short UV exposure. This reversible aging is attributed to the re-adsorption of oxygen, which for manufacturing reasons is trapped at the interface of ZnO, even in an oxygen-free environment. This oxygen can be removed with a UV pretreatment of the ZnO but at the expense of device efficiency and production that has to take place in an oxygen-free environment. This study establishes that stability measurements of ZnO-containing OSCs must be performed exclusively with a light source including a UV part since the usage of a simple white light source – as often reported in the literature – can lead to erroneous results.

1. Introduction

Zinc oxide (ZnO) is one of the most popular and widely used electron transport materials in organic solar cells, owing to its many advantageous properties, such as high transparency, conductivity and stability, low cost and toxicity, and easy solution-based processing.[1,2] On the other hand, however, ZnO is also a complex material with a pronounced defect chemistry, whose electronic properties strongly depend on processing conditions and environment. One of its major problems is the so-called light-soaking issue.[3] ZnO-containing solar cells need exposure to light with an energy corresponding to the ZnO band gap – usually in the ultraviolet (UV) range – to reach their full potential.[4,5] Without this light-soaking, the current-voltage characteristics show an s-shape with a reduced fill factor (FF) and an increased serial resistance, as schematically shown in **Figure 1** with the red curve. The necessary exposure time and wavelength of light depend on the exact properties of the used ZnO but are usually in the range of some seconds and between 360–380 nm, respectively. Importantly, the light-soaking issues are reversible, meaning that after some time without UV illumination, the cell performance can degrade again with the s-shape and reduced fill factor coming back. The cause of the light-soaking issues is attributed to oxygen being chemically adsorbed on the surface of zinc oxide, which traps negative charges at the surface of the ZnO and thus at the interface to the photoactive layer of the solar cell. This leads to an upward band bending toward the surface of the ZnO layer and consequently a hindered electron extraction, resulting in enhanced interface recombination and a decreased FF. UV irradiation generates electron-hole pairs in the ZnO, of which the holes can recombine with the trapped electrons, leading to desorption of the oxygen and a reduced band bending. Consequently, the electron extraction issue at the interface of active layer and ZnO is resolved.[5–7] However, irradiation with UV can also result in the generation of oxygen radicals which can decompose the absorbing layer, which is why the duration of UV illumination is usually kept as short as possible.[8–11]

Since oxygen is responsible for the light-soaking issues, they are especially pronounced in oxygen-containing atmospheres, where the FF is decreasing within several minutes without UV illumination due to oxygen diffusing through the active layer to the ZnO interface and adsorbing there.[4] On the contrary, the light-soaking issues are strongly reduced in an oxygen-free environment (e.g., a glove box) and it can be reasonably

M. Günther, S. S. Rivas, D. Blätte, T. Bein, T. Ameri
Department of Chemistry and Center for NanoScience (CeNS)
Ludwig-Maximilians-Universität (LMU)
Butenandtstr. 5-13, 81377 Munich, Germany
E-mail: tayebeh.ameri@ed.ac.uk

S. Lotfi, J. P. Hofmann
Surface Science Laboratory
Department of Materials and Earth Sciences
Technical University of Darmstadt
Otto-Berndt-Strasse 3, 64287 Darmstadt, Germany

T. Ameri
Institute for Materials and Processes
School of Engineering
University of Edinburgh
Sanderson Building, Edinburgh EH9 3FB, UK

The ORCID identification number(s) for the author(s) of this article can be found under https://doi.org/10.1002/adfm.202209768.

**ADVANCED
SCIENCE NEWS**

www.advancedsciencenews.com

**ADVANCED
FUNCTIONAL
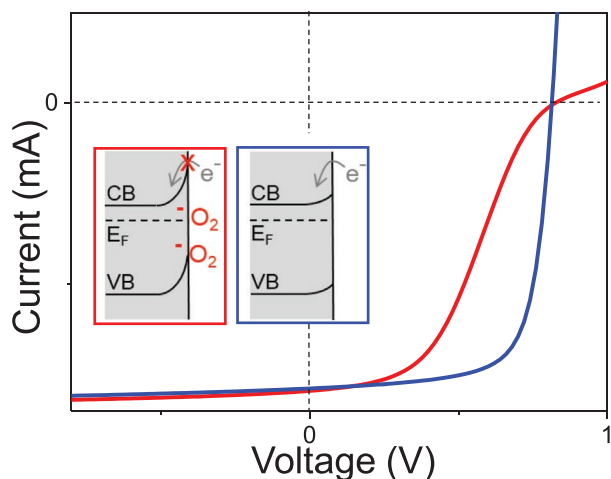MATERIALS**

www.afm-journal.de

Figure 1. Schematic current-voltage curves for a ZnO-containing organic solar cell before (red) and after (blue) UV light-soaking. The insets show the valence band (VB), conduction band (CB), and Fermi-level (E_F) of the zinc oxide with adsorbed oxygen and upward band-bending (red), which hinders the electron injection from the active layer, and after the desorption of oxygen (blue) with decreased band-bending.

assumed that in such an atmosphere one short initial UV exposure is enough to resolve the light-soaking issues long-term.

This assumption is particularly important when it comes to stability measurements of ZnO-containing solar cells. Thermal stability or photostability of OSCs is often investigated in an oxygen-free atmosphere using a light source without UV part to determine the performance of the cells over time.[12–16] This is either done to distinguish UV-induced aging from other aging factors or it is for pragmatic or financial reasons since it is by far easier and cheaper to do long-term aging with a white light LED, which has a stable intensity and only needs little cooling, in contrast to expensive xenon-lamp solar simulators.

In this work, we show that the influence of ZnO light-soaking cannot be neglected even in an oxygen-free atmosphere and that, therefore, investigations on thermal or photostability can be misleading under such conditions. We demonstrate for several different active materials that stability measurements of ZnO-containing solar cells which are performed with a light source without a UV component in an oxygen-free atmosphere show a reversible degradation that can be recovered completely by a short UV treatment. This reversible degradation is amplified at elevated temperatures, which makes it prone to be mistaken for thermal degradation of the solar cell. Using X-ray photoelectron spectroscopy (XPS) measurements, we show that the reversible degradation is caused by oxygen, which is unavoidably trapped at the interface between ZnO and the active layer, and which re-adsorbs on the ZnO thermally activated, resulting in a hindered electron extraction and a decreased fill factor.
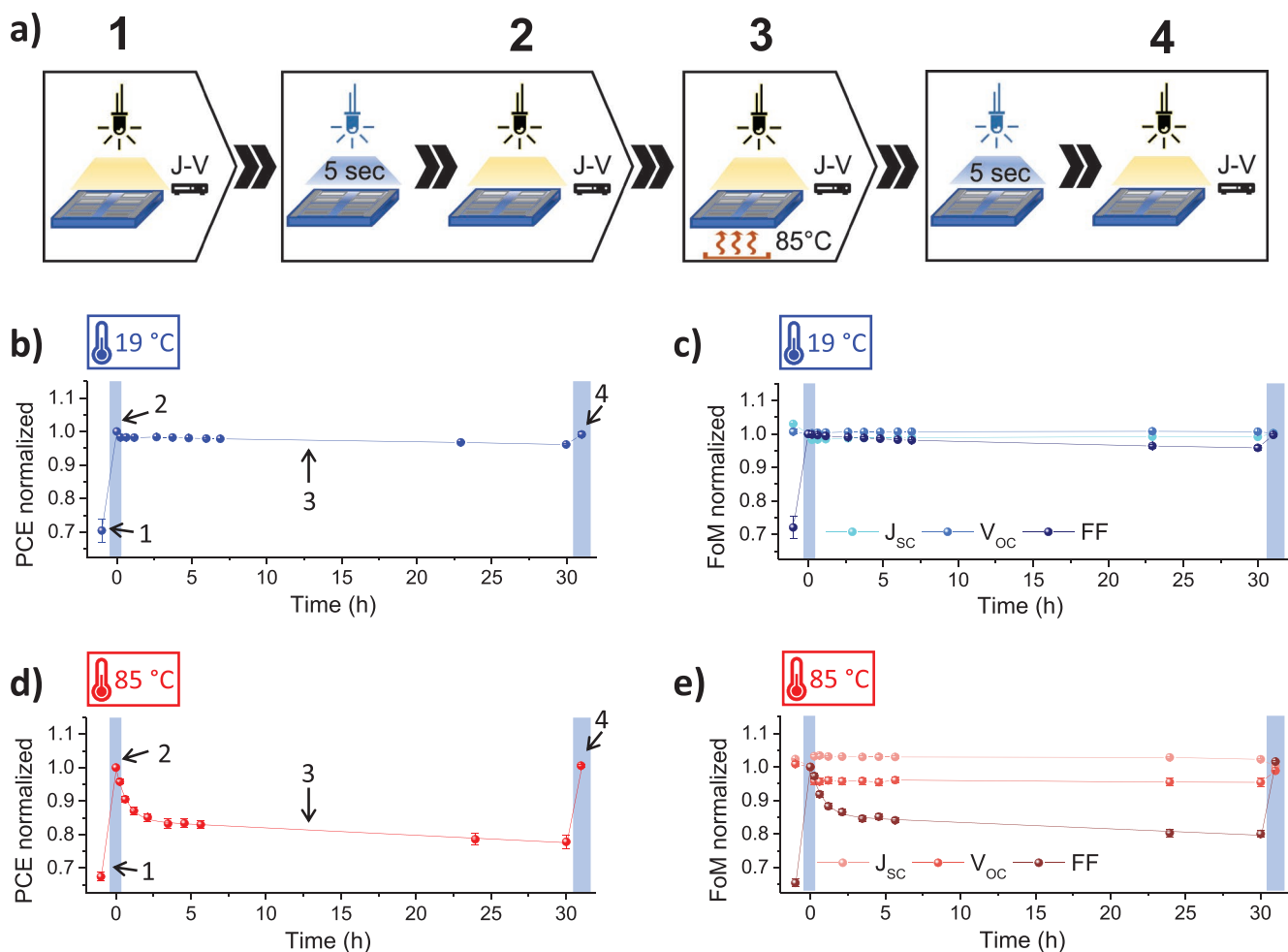
2. Results and Discussion

In order to study the influence of ZnO light-soaking issues on thermal stability measurements, inverted organic solar cells with an architecture ITO|ZnO (30–40 nm)|active layer (80–100 nm)|MoO$_x$ (10 nm)|Ag (100 nm) were built, containing

the active layer materials PBDB-TF and IT-4F at a 1:1 weight ratio. The molecular structures and a scheme of the cell architecture can be found in Figure S1 (Supporting Information). The commercially available ZnO nanoparticle dispersion (2.5 wt.% in 2-propanol) was spin-coated on ITO substrates, annealed at 120 °C for 10 min in air, and subsequently transferred into a nitrogen-containing glove box in which the spin coating of the active layer and the evaporation of MoO$_x$ and Ag was carried out. The finished cells were then subjected to the measurement routine schematically depicted in **Figure 2**a. All steps of this routine were performed in a nitrogen-containing glove box, with the cells having no further contact with oxygen.

First, current density-voltage (J–V) curves were measured for the freshly prepared cells with a white light LED (step 1 in Figure 2a) at room temperature (= 19°C). The used LED has a cut-off wavelength of 430 nm, thus containing no UV part, and was calibrated with a silicon photodiode to match the photocurrent under AM 1.5 (see Figure S2, Supporting Information for emission spectrum and experimental part for calibration details). The cells then were illuminated with a UV LED for 5 s to overcome the light-soaking issues and a second J–V curve was measured with the white light LED (step 2 in Figure 2a). The UV LED with a wavelength of 365 nm was calibrated with a silicon photodiode to match the UV part of AM 1.5G (=4.6 mW m^{-2}). The spectrum of the UV LED is also shown in Figure S2 (Supporting Information). After those two initial J–V measurements, the cells were subjected to thermal aging on a hotplate for 30 h at 85 °C, being kept in the dark except for J–V measurements performed at regular intervals with the white light LED (step 3 in Figure 2a), which is in accordance with the typical procedure in the literature for thermal aging.[17,18] To examine whether the absence of a UV component had an influence on the measurement results during the 30 h of thermal aging, the cells were then again illuminated with the UV LED for 5 s, and a final J–V measurement was taken with the white light LED (step 4 in Figure 2a).

For better comparability, the performance data of all cells measured with this procedure and presented below are normalized to the respective cell's performance after the initial 5 s UV-soaking (step 2). All presented data points are averaged over six independently measured cells. The freshly prepared PBDB-TF:IT-4F cells in general showed the expected strong s-shape in step 1 due to the missing UV soaking, with a low fill factor of 46.0 ± 1.0%, a low power conversion efficiency (PCE) of 6.8 ± 0.4%, an open-circuit voltage (V_{OC}) of 0.80 ± 0.05 V, and a short-circuit current density (J_{SC}) of 18.8 ± 0.7 mA cm^{-2} (average over all measured cells). After the initial 5 s UV-soaking in step 2, the performance improved to an average PCE of 11.8 ± 0.3%, a FF of 73.5 ± 0.2%, a V_{OC} of 0.84 ± 0.01 V, and a J_{SC} of 18.7 ± 0.4 mA cm^{-2}. These values are a bit lower than the 12–13% PCE which are usually reported in the literature for inverted PBDB-TF:IT-4F cells,[8,19] however, since the aim of this project was a deeper understanding of the stability behavior, the cells were not further optimized.

The results of the J–V measurements performed with the described routine for reference cells kept at room temperature (19 °C) are shown in Figure 2b,c. After the initial UV soaking, the cells show a relatively constant PCE over time, however, after 30 h, a small relative loss of ≈4% in PCE is apparent,

Figure 2. a) Scheme depicting the measurement procedure used. The whole procedure is performed in an oxygen-free environment and at 19 °C if not otherwise stated. As a first step, a J–V curve is measured of the pristine cells with a white light LED, followed by a 5 s UV illumination (365 nm) and another J–V measurement with the white light LED (step 2). Then the cells are thermally aged for 30 h at 85 °C and measured at regular time intervals with the white light LED (step 3). As a last step, the cells are again illuminated with UV light for 5 s and measured. b,c) Normalized performance as a function of time for the different figures of merit (FoM) of PBDB-TF:IT-4F solar cells, which were measured according to the described procedure but as were kept at 19 °C in step 3 as a reference. The blue markings indicate the time of the UV treatments. d,e) Normalized performance as a function of time for PBDB-TF:IT-4F cells measured at 85 °C according to the described procedure.

which can be attributed to a decreasing FF, while J_{SC} and V_{OC} are stable over time. Notably, this small loss is fully recovered after the final 5 s of UV illumination, showing that it is not a real thermal aging effect. Thus, already the behavior at room temperature is an indication that the absence of UV illumination can produce erroneous stability results. Nevertheless, the influence is relatively small and can probably be justifiably neglected on the chosen timescale, especially if other aging influences are responsible for much larger losses.

However, the behavior over time changes drastically when the cells are thermally aged at a temperature of 85 °C (Figure 2d, e), which is the commonly used condition for thermal stability tests.[17] After the initial UV soaking, the cells' performance shows a strong exponential decay, with a relative PCE loss of 15% already after two hours. After ≈20 h, >20% of the initial efficiency is lost, exceeding the cell's lifetime according to the T_{80} definition.[18] The PCE loss is mainly attributed to the decreasing FF, while the J_{SC} and V_{OC} are

constant over time with a small initial increase and decrease, respectively, which is due to the J–V measurement being performed at elevated cell temperature. Strikingly, here again, the final UV soaking step recovers all of the losses and restores the initial cell performance, clearly proving that the cells did not thermally degrade during the measurement time. In fact, after the second UV soaking, the PCE is even ≈1% higher compared to the initial value, which we attribute to a long-term annealing effect on our devices. This means that the usage of a white light source without a UV part for characterizing cells at elevated temperatures resulted in a PCE loss, that could be wrongly attributed to thermal degradation, but is fully recoverable by UV illumination.

Hence, the main question is why the lack of a UV illumination component, especially at elevated temperatures, leads to a decrease in cell performance. Two causes would seem plausible: The behavior could originate from the active layer, for example, when thermal degradation is cured by UV
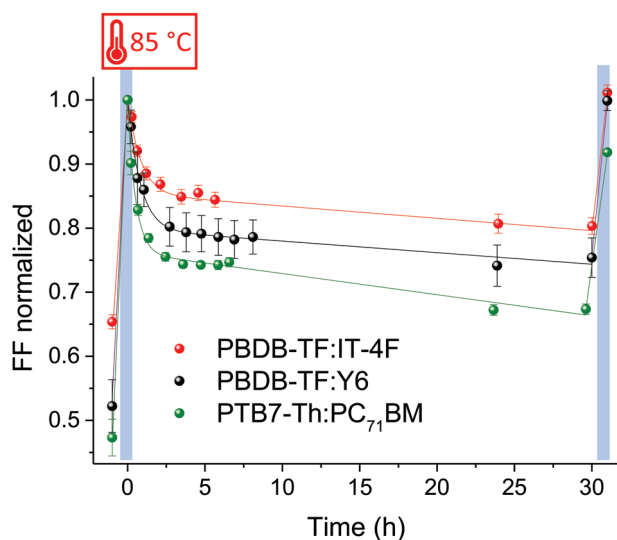
Figure 3. Normalized fill factor as a function of time for the three different active layers PBDB-TF:IT-4F (red), PBDB-TF:Y6 (black), and PTB7-Th:PC$_{71}$BM (green). The measurements were run according to the procedure described in Figure 2a, with the first data point being the pristine cells, the second data point (blue marking) being the UV-soaked cells, followed by thermal aging at 85 °C, and the last data point representing the cells that were again soaked with UV-light (blue marking).

illumination, although this would be rather unusual for organic solar cells. Or the behavior could be caused by the interfacial layers, in which case ZnO light-soaking issues would be an apparent possibility.

To investigate whether the active layer is responsible for this behavior, cells with two alternative active layers – one being PTB7-Th:PC$_{71}$BM and one being PBDB-TF:Y6 (systematic molecule names can be found in the experimental part; the structures are shown in Figure S3, Supporting Information) – were prepared with the otherwise same cell architecture and subjected to the same measurement procedure at 85°C. The behavior of the FF over time for the different active layers is shown in **Figure 3**. Again, all values are normalized to the performance after the initial UV-soaking and averaged over six independently measured cells. The corresponding graphs for PCE, V_{OC}, and J_{SC} can be found in Figure S4 (Supporting Information). For all three different active layers, a clear degradation of the FF after the initial UV-soaking occurs, with a comparable, exponential decay in the first few hours. For PBDB-TF:IT-4F and PBDB-TF:Y6, the initial performance can be fully restored with the UV-soaking step after 30 h. For PTB7-Th:PC$_{71}$BM, the performance is only partly restored. This can probably be explained by real thermal aging of the active layer, as PBT7-Th:PC$_{71}$BM blends are known to phase-separate at elevated temperatures, resulting in a decreased FF and PCE.[20]

Since the used alternative active layers show a comparable behavior to the initial PBDB-TF:IT-4F system, although they exhibit both molecularly and morphologically major differences, it seems to be very unlikely that those materials are responsible for the observed behavior. Instead, it is much more likely that this reversible thermal degradation originates from the interface layers. And indeed, a very similar behavior originating from ZnO light-soaking is well-known in the

literature:[4,5] When ZnO-containing cells with a protective UV filter are measured in air, their performance degrades within several minutes, with the J–V curve developing a strong s-shape with reduced FF and increased serial resistance. When the UV filter is removed, the performance can be fully recovered. This behavior is attributed to oxygen diffusing into the cell and adsorbing on the ZnO interface with the active layer, resulting in band bending and hindered electron extraction. Illuminating the cell with UV light results in immediate desorption of oxygen and thus in a recovered performance.

In contrast to those literature reports, however, the measurements in this work were carried out under exclusion of oxygen and at elevated temperatures. The question is therefore whether the observed behavior nevertheless can be explained by the adsorption of oxygen and where this oxygen comes from in an oxygen-free atmosphere.

To answer this question, the used ZnO layer was examined in more detail. The layer consists of commercially available ZnO nanoparticles, which are highly crystalline with the typical wurtzite crystal structure, as confirmed by the powder X-ray diffraction (XRD) pattern shown in **Figure 4**a. From the reflection line broadening an approximate particle size of 12 nm is calculated with the Scherrer equation. As apparent from the atomic force microscopy (AFM) image in Figure 4b, the spin-coated and annealed ZnO films consist of closely packed nanoparticles with very good coverage, exhibiting a smooth surface with a low roughness of 0.86 nm root mean square. From the UV–vis spectra of the ZnO film and the active layer PBDB-TF:IT-4F shown in Figure 4c it is evident that the spectral range of the UV LED is mainly absorbed by the ZnO, while the active layer primarily absorbs in the visible range.

In order to obtain more information about the chemical speciation of possibly adsorbed oxygen on the surface, the ZnO layer was investigated with X-ray photoelectron spectroscopy (XPS). As expected, mainly the elements zinc and oxygen are visible in the survey spectrum, which is shown in Figure S5 (Supporting Information). In addition, however, carbon is detectable, which indicates organic impurities, for example, residues of spin coating the ZnO nanoparticles from 2-propanol or adventitious carbon species adsorbed from handling the samples in ambient conditions. In Figure 4d the high-resolution scan of the O 1s region is shown. According to literature, the spectrum was fitted with three components corresponding to stochiometric O^{2-} ions in the wurtzite structure (O$_{st}$, 530.0 eV), O^{2-} ions in oxygen-deficient regions of the wurtzite structure (O$_{def}$, 531.0 eV), and adsorbed oxygen species (O$_{ads}$, 532.2 eV).[21–23] The latter might be atmospheric oxygen which is physisorbed or chemisorbed as oxygen atoms or molecules, depending on temperature and atmospheric composition.[6,24] The details of assigning this species are a controversial topic in literature, but below 150°C and in an ambient atmosphere chemisorbed O$_2^-$ seems to be the dominating species.[24] Additional adsorbed oxygen species coming from sources other than atmospheric oxygen may also be involved, such as CO$_x$, -OH, or H$_2$O. However, due to the close-lying O 1s binding energies of the different possible adsorbates in the 532–533 eV region it is not possible to unambiguously identify the molecular nature of the O-containing adsorbate. Notably, the adsorbed species is stably present and neither affected nor
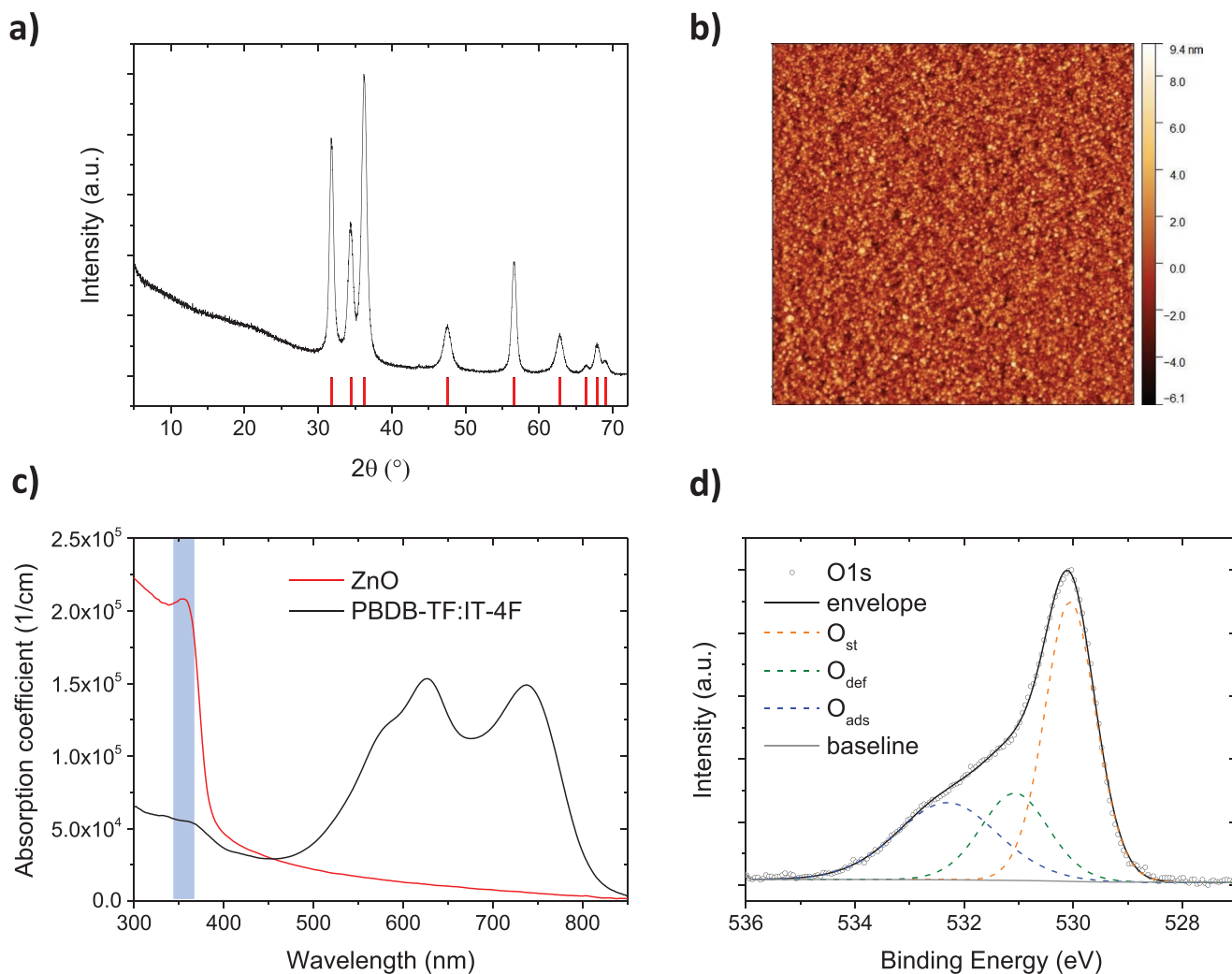
Figure 4. a) Powder X-ray diffractogram of the used ZnO (black line) with red bars indicating the diffraction lines of ZnO hexagonal wurtzite structure. b) Atomic force microscopy image of the ZnO layer surface, showing densely packed ZnO nanoparticles with a root mean square (RMS) roughness of 0.86 nm. c) UV–vis absorption spectra of a ZnO film (red line) and a PBDB-TF:IT-4F film (black line) on a quartz substrate, respectively, with the blue bar indicating the emission range of the used UV-LED. d) O 1s XPS spectrum of the ZnO layer, fitted with three components for stoichiometric oxygen (O_{st}) of bulk ZnO, oxygen in oxygen-deficient regions (O_{def}), and adsorbed oxygen species (O_{ads}). The black line represents the envelope of the fitted components.

desorbed by sample storage in an N_2 glove box nor by handling in ultra-high vacuum conditions during XPS analysis.[21]

Based on the results presented so far, we hypothesize the following: The freshly prepared solar cells contain an adsorbed layer of oxygen species on top of the zinc oxide layer, which is unavoidable due to the necessary manufacturing of the ZnO layer in air, even if all other steps are performed in an oxygen-free atmosphere. The oxygen-containing adsorbates then are enclosed by the active layer spin-coated on top and cause an upward band bending in the ZnO. The initial UV treatment or the first illumination of the pristine cells with a UV containing AM 1.5G spectrum results in desorption of those oxygen species and thus in good cell performance. However, due to the active layer being on top of the ZnO, the desorbed oxygen species are confined at the interface and therefore are able to re-adsorb. The adsorption of oxygen onto ZnO is known to be an endothermic process, where the activation energy strongly depends on the exact ZnO layer properties and environmental conditions.[25,26] Therefore, the elevated temperature of 85°C accelerates the re-adsorption and thus also speeds up the performance loss, while at room temperature the re-adsorption and the resulting degradation are very slow.

To verify this hypothesis, thermal stability was measured at several temperatures for eight hours with the procedure described in Figure 2a. In case the hypothesis is correct, the thermal degradation should show a strong, consistent temperature dependence and it should be possible to determine apparent activation energy from the temperature-dependent decay time constants. And indeed, as shown in **Figure 5a** the fill factor follows an exponential decay over time for all tested temperatures, with the slope of this decay increasing with temperature. For all degradation temperatures, after eight hours, the FF could be fully restored by a 5 s UV illumination (measurement points at 8 h, blue marking in Figure 5a). Interestingly, the cells
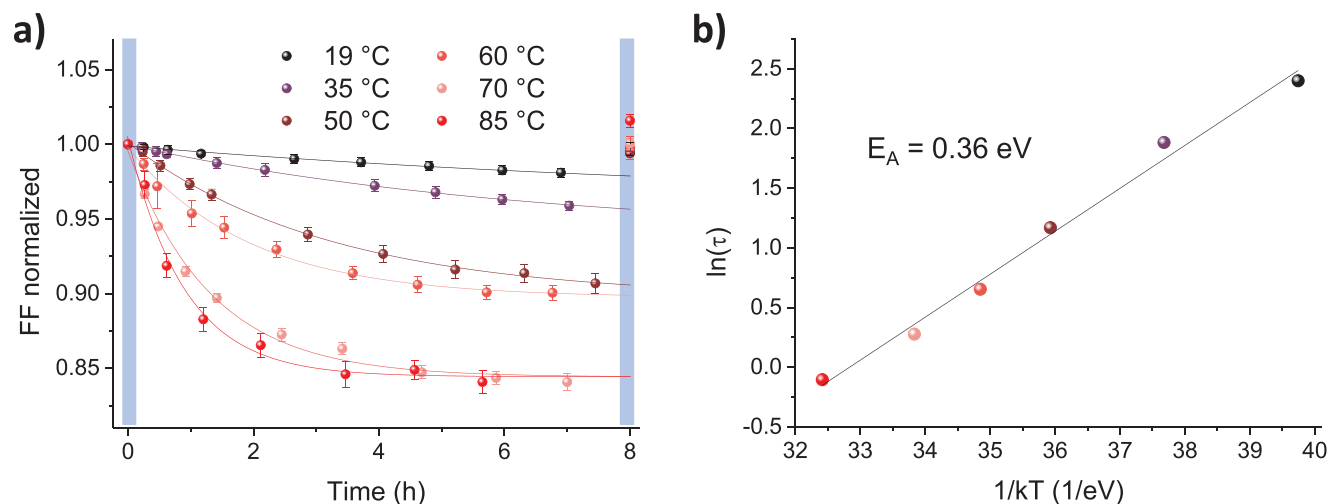
Figure 5. a) Development of the normalized fill factor as a function of time for PBDB-TF:IT-4F devices heated at different temperatures between 19 °C and 85 °C, with the data points being the average of five separately aged solar cells. All values are normalized to the initial performance after 5 s of UV illumination (time = 0, blue marking) and after 8 h of thermal degradation, the devices were exposed to a second UV illumination of 5 s (blue marking). The exponential fits of the respective data points according to Equation 1 are shown as solid lines. b) Semi-logarithmic Arrhenius-type diagram of the time constants obtained from the exponential fits over the inverse temperature T multiplied with the Boltzmann constant k. The linear fit of the data is indicated with a solid black line, with the fit's slope corresponding to the activation energy $E_A = 0.36$ eV.

measured at 85 °C even show a small improvement in performance after the re-soaking compared to the freshly UV-soaked cells, which probably can be attributed to a beneficial annealing effect on the active layer morphology. To obtain the decay time constant τ, the measurement data of the fill factor over time FF(t) for each temperature was fitted with an exponential decay with offset y_0 and scaling factor A according to Equation 1:

$$FF(t) = y_0 + A \cdot \exp\left(-\frac{t}{\tau}\right) \qquad (1)$$

The use of FF(t) for this fit can be justified by the fact that the FF is the parameter that should be most sensitive to possible band bending at the ZnO interface and therefore should have a direct linear correlation to the amount of adsorbed oxygen species. The corresponding data for V_{OC}, J_{SC}, and PCE over time and the details for all fits can be found in Figure S6 and Table S1 (Supporting Information). The obtained time constants then were plotted semi-logarithmically in an Arrhenius-type diagram versus the inverse temperature, as shown in Figure 5b. The linear trend of the data points is clearly evident, indicating that the temperature-dependent behavior is indeed controlled by one process with uniform activation energy. More importantly, from the slope of the linear fit, apparent activation energy can be determined with a value of $E_A \approx 0.36$ eV. There are no literature values for the activation energy of oxygen adsorption on ZnO within a solar cell, however, there are values for this process on pure ZnO nanowires. Madel et al.[25] investigated the persistent photoconductivity of ZnO nanowires and found an activation energy of 0.16 eV for oxygen adsorption in a pure oxygen atmosphere. For a lower atmospheric oxygen content, the activation energy was found to increase, with a value of 0.33 eV in an atmosphere with 1% oxygen in argon. In comparison, for the case investigated here, an activation energy of 0.36 eV seems to match this trend, considering that there

is no atmospheric oxygen but only the oxygen trapped at the interface.

Provided that the presented hypothesis is correct, the problem of thermal degradation should be solvable by removing the oxygen species adsorbed on the ZnO by UV illumination before the additional solar cell layers are deposited.

To this end, we transferred freshly prepared ZnO layers into a nitrogen-filled glove box and exposed them to UV illumination for different time periods before depositing the other layers and avoiding any further contact with oxygen, analogous to the approach described by Liu et al.[27] which they used to reduce photocatalytic decomposition of active layer materials by oxygen adsorbed on ZnO. The cells pretreated in this way then were exposed to the same procedure as described in Figure 2 and heated at 85°C for 30 hours. The resulting normalized PCE and FF over time for no pretreatment and pretreatments of 2 min, 10 min, and 1 h are shown in **Figure 6**a,b, the corresponding trends for J_{SC} and V_{OC} can be found in Figure S7 (Supporting Information).

It is clearly visible that the FF loss is greatly reduced even for a ZnO pretreatment of 2 min compared to the untreated devices. A pretreatment of 10 min almost completely eliminates the degradation within this time frame, with a total loss in PCE of ≈2% after 30 h. An even longer pretreatment time of up to one hour did not show any further improvement, which is why 10 min of UV treatment is assumed to be the optimum at the used UV light intensity.

To understand how exactly the UV pretreatment affects the ZnO surface, a ZnO layer was illuminated with UV inside the XPS chamber and the O 1s spectrum was recorded before and after the illumination (technical details can be found in the experimental section). The corresponding min-max normalized O 1s spectra are shown in Figure 6c. As described above, both spectra were fitted with three components for stochiometric oxygen (O_{st}), oxygen in oxygen-deficient regions (O_{def}),
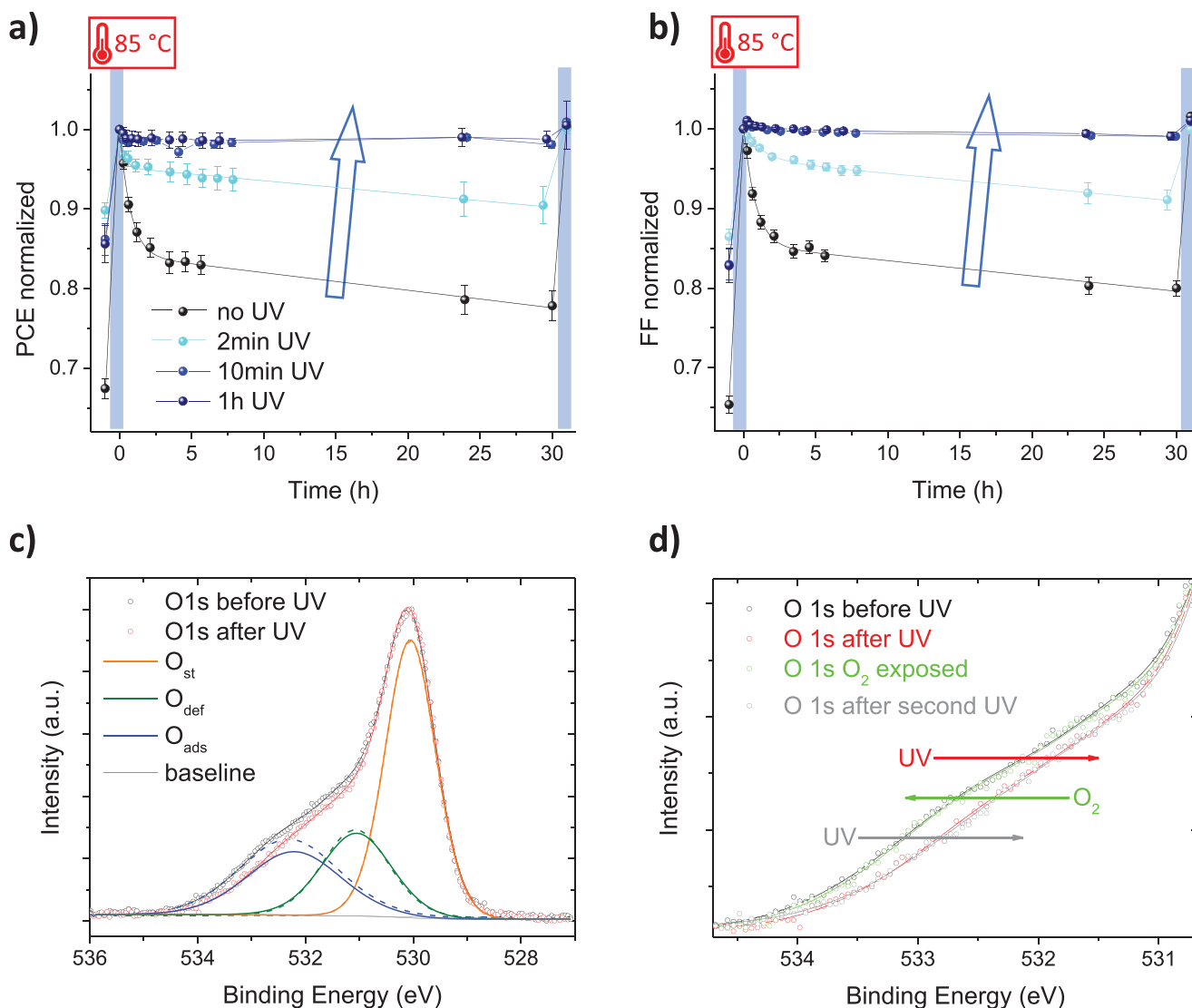
Figure 6. a) Normalized PCE and b) FF as a function of time for PBDB-TF:IT-4F solar cells, for which the ZnO was illuminated with UV light at different times as a pretreatment. The measurements were run according to the procedure described in Figure 2a, with the first data point being the pristine cells, the second data point being the UV-soaked cells (blue marking), followed by thermal aging at 85 °C, and the last data point showing the cells that were again soaked with UV-light (blue marking). c) O 1s XPS spectra for a ZnO layer before (black) and after (red) UV illumination inside of the XPS chamber. The spectra were fitted with three components for the stochiometric oxygen (O_{st}), the oxygen in oxygen-deficient regions (O_{def}), and adsorbed oxygen species (O_{ads}), dashed lines and solid lines representing the fits for the spectrum before and after illumination, respectively. d) Enlarged high binding energy region of O 1s spectra for the ZnO layer before (black) and after (red) UV illumination and after oxygen exposure (green) and a second UV illumination (gray).

and adsorbed oxygen species (O_{ads}). As to be expected, the O 1s spectrum shows no difference due to the UV treatment in the region of the stochiometric oxygen signal. However, the illumination reduces the signal intensity in the region between 531–534 eV, which can be mainly assigned to a reduction of the adsorbed oxygen species, supporting the concept of UV-induced desorption. For a quantitative evaluation, the non-normalized fits of the three components were integrated and the percentage of each component in the total O 1s integral was calculated (see Table S2 Supporting Information). The component for adsorbed oxygen species accounts for 27% before UV illumination and 22% afterward, showing a significant reduction.

To get an idea of which oxygen species are involved in the desorption and re-adsorption process, following the first UV illumination of the ZnO layer, the sample was exposed to an O_2 partial pressure of 0.1 mbar in the same vacuum system and a third O 1s spectrum was recorded. Afterward, the ZnO layer was UV illuminated a second time and a final O 1s spectrum was obtained. A comparison of those four O 1s spectra in the relevant region between 531–534 eV is shown in Figure 6d.

It is clearly visible that the oxygen exposure again results in the same spectrum as for the ZnO layer before illumination, while the second illumination reproduces almost the same spectrum after the first illumination. We take this as proof that the observed behavior of the corresponding solar cells is

ADVANCED
SCIENCE NEWS
www.advancedsciencenews.com

ADVANCED
FUNCTIONAL
MATERIALS
www.afm-journal.de

Table 1. Work function (WF), valence band maximum (VB), and conduction band minimum (CB) of a ZnO layer before and after UV illumination obtained from UV photoelectron spectroscopy.

	WF [eV]	VBM [eV]	CBM [eV]
Before UV	3.69	−7.00	−3.63
After UV	3.65	−7.03	−3.66

Table 2. Averaged performance parameters for pristine PBDB-TF:IT-4F cells for different ZnO pretreatment times (J–V measurement performed after 5 s of UV soaking to achieve maximum performance).

ZnO treatment	J_{SC} [mA cm^{-2}]	V_{OC} [V]	FF [%]	PCE [%]
none	18.7 ± 0.4	0.84 ± 0.01	73.5 ± 0.2	11.8 ± 0.3
2min	18.3 ± 0.6	0.83 ± 0.01	73.5 ± 0.4	11.1 ± 0.5
10min	18.1 ± 0.6	0.82 ± 0.01	73.0 ± 0.1	10.8 ± 0.4
1h	18.1 ± 0.6	0.81 ± 0.01	73.0 ± 0.3	10.7 ± 0.3

governed by the reversible desorption and re-adsorption of molecular oxygen, while the other adsorbed oxygen species do not interfere with the cell's performance. However, we note that when fitting the O1s spectra, the weighting between O$_{ads}$ and O$_{def}$ is not unambiguous. Another interpretation is also possible, where the observed changes could be partly attributed to a change in oxygen speciation in the oxygen-deficient region. Nevertheless, we consider the simple, reversible desorption and re-adsorption of oxygen to be the chemically more plausible process and therefore chose the presented fitting.

Furthermore, to confirm experimentally that the adsorption and desorption of oxygen indeed change the work function of the ZnO surface, we performed UV photoelectron spectroscopy (UPS) on a ZnO layer before and after illuminating the ZnO with UV light inside the UPS analysis chamber, analogous to the XPS measurements. The resulting UPS spectra of the valence band region and the secondary-electron cut-off region (SEC, measured with a bias of 8 eV) of a ZnO layer before and after UV illumination can be found in Figure S8 (Supporting Information). A linear method (extrapolation of the leading edge to the zero baselines of VBM and SEC) was used to obtain the values of SE energy cut-off and VBM. The low binding energy onset in the valence band region provides the energetic distance between valence band maximum (VBM) and Fermi level. With a literature value of 3.37 eV for the ZnO band gap,[28] the conduction band minimum (CBM) and valence band energies versus vacuum can be calculated, as summarized in **Table 1**. It is evident that the UV illumination results in a small but consistent down-shift of the ZnO energy levels by ≈30 meV. It must be mentioned that by illuminating ZnO with UV, the charge carrier density in the material is increased. After the end of illumination, this higher charge carrier density decreases only slowly due to the so-called persistent photoconductivity of ZnO. [29] This phenomenon to a small extent could also influence the UPS measurements. However, in combination with the above-explained XPS results, those UPS results further support the hypothesis that the UV-induced desorption of oxygen reduces the band bending at the ZnO interface, resulting in improved electron injection from the active layer to ZnO, and thus in an increased fill factor.

To summarize, the UV pretreatment of the ZnO layer eliminates the problematic reversible degradation behavior, but it is not a flawless solution, since the pretreatment itself decreases the device efficiency. The performance parameters of the pristine cells after the initial 5 s UV-soaking are listed in **Table 2** for different ZnO pretreatment times. All figures of merit decrease with the duration of the ZnO pretreatment, with a drop of PCE from 11.8% (untreated) to 10.8% for the optimum time of 10 min pretreatment. The cause of this loss is not clearly attributable, but it seems reasonable that by changing

the surface chemistry of ZnO through UV pretreatment (e.g., the dipole moment of the interface), the behavior of the devices are also affected. However, a small and time-independent loss in PCE after a ZnO pretreatment (≈8% of relative PCE loss for 10 min UV pretreatment) is certainly preferable to a progressive thermal degradation, which means a loss of >20% after only 30 h.

3. Conclusion

In conclusion, we have studied the influence of ZnO light-soaking on stability measurements of inverted organic solar cells. It was found that the inverted devices in the absence of UV illumination show a reversible degradation of performance, mainly governed by a loss of FF, which can be recovered by a short UV illumination. Such behavior is principally known for OSCs with ZnO as ETL and is usually explained by the fact that atmospheric oxygen diffuses through the cells and adsorbs on the ZnO surface, resulting in an upward band bending in the ZnO, which hinders electron extraction and thus decreases FF and PCE. UV illumination helps desorbing the oxygen and thus recovers the performance. In this work, however, we show that this kind of reversible degradation unexpectedly also occurs in an oxygen-free environment and is amplified by higher temperatures. We hypothesize that instead of oxygen diffusing in from the atmosphere, the cause of the reversible degradation here is oxygen that is already adsorbed on the ZnO surface due to its production process. Although this oxygen can be desorbed with an initial UV treatment, it is then trapped at the interface between ZnO and active layer and can re-adsorb when no continuous UV illumination is applied. As evidence, we show that the reversible degradation is independent of the used active layer materials and that its temperature dependence can be attributed to the activation energy of oxygen re-adsorption. Finally, we demonstrate, supported by XPS measurements, that removing the oxygen from the ZnO surface by a UV pretreatment before building the solar cell solves the reversible degradation problem, however, at the price of a small loss of device efficiency.

This work establishes that stability measurements of ZnO-containing OSCs should be performed exclusively with light sources featuring a UV part and closely reproduce the AM 1.5G spectrum, otherwise there is a high risk of confusing real aging effects with ZnO light-soaking effects. Furthermore, there are additional implications for using ZnO in commercial OSCs: since the oxygen is typically adsorbed on the ZnO due to the manufacturing process, its presence cannot be avoided even by

**ADVANCED
SCIENCE NEWS**

www.advancedsciencenews.com

**ADVANCED
FUNCTIONAL
MATERIALS**

www.afm-journal.de

encapsulating the assembled cells. However, the oxygen present reduces the performance of the solar cells under operation, especially in the morning hours when the UV component in natural sunlight is not yet sufficient for complete oxygen desorption. This could only be avoided by pretreating the ZnO layer with UV and performing the whole manufacturing process under complete exclusion of oxygen. It is likely that such increased manufacturing cost and complexity could lead to a re-assessment of the utility of ZnO to serve as ETL in commercial OSCs.

4. Experimental Section

Materials: ITO substrates with a sheet resistance of 15 Ω cm^2 were purchased from Kintec. The ZnO nanoparticle dispersion (N-10) was obtained from Avantama AG. Poly[(2,6-(4,8-bis(5-(2-ethylhexyl)thiophen-2-yl)-benzo[1,2-b:4,5-b']dithiophene))-alt-(5,5-(1',3'-di-2-thienyl-5',7'-bis(2-ethylhexyl)benzo[1',2'-c:4',5'-c'] dithiophene-4,8-dione)]   (PBDB-TF),   3,9-bis(2-methylene-((3-(1,1-dicyanomethylene)-6,7-difluoro)-indanone))-5,5,11,11-tetrakis(4-hexylphenyl)-dithieno[2,3-d:2',3'-d']-s-indaceno[1,2-b:5,6-b'] dithiophene (IT-4F) and 2,2″-((2Z,2″Z)-((12,13-bis(2-ethylhexyl)-3,9-diundecyl-12,13-dihydro-[1,2,5]thiadiazolo[3,4-e]thieno[2″,3″:4',5″] thieno[2″,3″:4,5]pyrrolo[3,2-g]thieno[2″,3″:4,5]thieno[3,2-b]indole-2,10-diyl)bis(methanylylidene))bis(5,6-difluoro-3-oxo-2,3-dihydro-1H-indene-2,1-diylidene))dimalononitrile (Y6) were purchased from Solarmer. Poly[4,8-bis(5-(2-ethylhexyl)thiophen-2-yl)benzo[1,2-b;4,5-b'] dithiophene-2,6-diyl-alt-(4-(2-ethylhexyl)-3-fluorothieno[3,4-b]thiophene-)-2-carboxylate-2-6-diyl)] (PTB7-Th) was obtained from 1-Material. [6,6]-Phenyl-C71-butyric acid methyl ester (PC$_{71}$BM, 99.5%) was purchased from Solaris Chem. Chlorobenzene (anhydrous, 99.8%), chloroform (anhydrous, >99%, amylene stabilized), 1,8-diiodooctane (DIO), and MoO$_3$ powder (99.97% trace metals basis) were purchased from Merck. 1-chloronaphthalene was obtained from TCI.

Device Fabrication: The ITO substrates were cleaned with detergent and ultrasonicated in water, acetone, and 2-propanol for 10 min. They were dried with a nitrogen flow and plasma-cleaned for 10 min. Subsequently, the ZnO nanoparticle dispersion was spin-coated with 1400 rpm for 45 s and annealed for 10 min at 120 °C in air. The substrates then were transferred into a nitrogen glovebox (oxygen level <0.1 ppm) and all following steps and measurements were performed without any further contact with oxygen, if not otherwise stated. For the active layer solutions, the components were separately dissolved in the respective solvent, followed by mixing and stirring overnight. The respective additive was added 30 min before spin coating. PBDB-TF:IT-4F solutions were prepared with a 10:10 mg mL^{-1} weight ratio in chlorobenzene with 0.5 vol% DIO and dynamically spin-coated at 900 rpm for 5 s and 4000 rpm for 60 s. For PTB7-Th:PC$_{71}$BM, a ratio of 8:12 mg mL^{-1} in chlorobenzene with 3 vol% DIO was used, and the solution was dynamically spin-coated with 1500 rpm for 45 s. PBDB-TF:Y6 solutions were prepared with 7.25:8.75 mg mL^{-1} in chloroform with 0.5 vol% 1-chloronaphthalene and dynamically spin-coated with 3000 rpm for 30 s. Finally, 10 nm of MoO$_x$ and 100 nm of Ag were evaporated through a mask.

Characterization Techniques: J–V measurements were carried out in a nitrogen-filled glove box using a Keithley 2401 source-measure unit and a white light LED (Bridgelux), which was calibrated to 100 mW cm^{-2} with a silicon diode (Hamamatsu S1227-66BQ). The cells were illuminated through a shadow mask with a 6.25 mm^2 open area. Wide angle X-ray diffraction measurements were performed in transmission with an STOE STADI P diffractometer (Cu K$_{\alpha1}$, $\lambda = 1.5406$ Å) and a Ge(111) single crystal monochromator equipped with a DECTRIS solid state strip detector MYTHEN 1K. For the sample preparation, the ZnO dispersion was drop-cast on a heating plate at 120°C (same conditions as for the annealing of the spin-coated films) and the emerging powder was used. The ZnO crystal structure was assigned using the ICSD database.[30] AFM measurements were done with a NANOINK atomic force microscope in tapping mode. UV–vis spectra of thin films on quartz substrates were recorded in transmission with a PerkinElmer LAMBDA 1050 instrument with an integrating sphere. XPS measurements were performed in the cluster tool Darmstadt Integrated System for Solar Cell research (DAISY-SOL) using a Thermo Fisher Scientific Escalab 250 system equipped with a monochromatized Al Kα X-ray source (1486.6 eV) operated at 200 W power and 650 µm spot size. UPS measurements were performed with the same spectrometer; He I (21.22 eV) was used. The He pressure inside the analytic chamber was set up at 2.5×10^{-8} mbar. The XPS spectra were collected at a take-off angle of 90° with respect to the sample surface. All XPS region scans (O 1s, Zn 2p) were acquired with a pass energy of 10 eV, a step size of 0.05 eV, and a dwell time of 50 ms per measurement point. Survey spectra were obtained with a pass energy of 50 eV, a step size of 0.5 eV, and a dwell time of 50 ms. UPS valence band edge and secondary electron cut-off were acquired with a pass energy of 2.5 eV, a step size of 0.05 eV, and a dwell time of 100 ms. All XPS spectra were binding energy calibrated to the main C 1s peak with a value of 285.0 eV and the Fermi level of clean silver (Ar sputtered) was used to calibrate the UPS corresponding spectra. The Fermi level value was determined with a sigmoid fit and taking the position where the intensity was at 50%. The Fermi level of the cleaned silver was used to determine the instrumental resolution: 0.35 eV for XPS (pass energy of 10 eV) and 0.22 eV for UPS (pass energy of 2.5 eV). Measurements were carried out in ultra-high vacuum (UHV $\leq$ 1×10^{-9} mbar). For re-adsorption experiments, the sample was exposed to an oxygen partial pressure of 0.1 mbar inside a separate vacuum chamber with a base pressure of 1×10^{-8} mbar as a part of the cluster tool vacuum system, i.e., all transfer operations were done under UHV conditions (<1×10^{-9} mbar). Peak fitting was performed using a sum of Gaussian (70%) and Lorentzian (30%) lines, while the secondary electron background was subtracted utilizing the Shirley function using CasaXPS software version 2.3.25.[31]

Stability testing: All stability tests were done in a nitrogen-filled glovebox with oxygen and water levels <1 ppm. For thermal stability measurements, all devices were first put into a home-built metal sample holder and subjected to a J–V measurement at room temperature (19 °C). Then the devices in the sample holder were transferred to a temperature-controlled heating plate and J–V measurements were performed in regular intervals with the devices maintaining the chosen temperature. The UV soaking before and after the thermal stability measurements was performed with a 365 nm UV LED (Thorlabs Solis-365C) which was calibrated with a Si-diode (Hamamatsu) to match the UV part of AM 1.5G (4.6 mW cm^{-2}).

Statistical Analysis: All stability measurements in this work were statistically evaluated according to the following procedure: For each aging condition, twelve individual solar cells on one common substrate were prepared and measured over time. To ensure unbiased filtering of outliers, from those twelve cells, the six cells with highest PCE were chosen. Then, the figures of merit of those six cells were individually normalized to their respective value at time = 0 h. The normalized values were averaged, and the standard deviation (SD) was calculated, which is shown in the graphs as an error bar (mean ± SD).

Supporting Information

Supporting Information is available from the Wiley Online Library or from the author.

Acknowledgements

ADVANCED
SCIENCE NEWS

www.advancedsciencenews.com

ADVANCED
FUNCTIONAL
MATERIALS

www.afm-journal.de

Conflict of Interest

The authors declare no conflict of interest.

Data Availability Statement

The data that support the findings of this study are available from the corresponding author upon reasonable request.

Keywords

[1] R. M. Hewlett, M. A. McLachlan, *Adv. Mater.* **2016**, *28*, 3893.

[2] C. Liu, C. Xiao, W. Li, *J. Mater. Chem. C* **2021**, *9*, 14093.

[3] J. Kim, G. Kim, Y. Choi, J. Lee, S. Heum Park, K. Lee, *J. Appl. Phys.* **2012**, *111*, 114511.

[4] M. R. Lilliedal, A. J. Medford, M. V. Madsen, K. Norrman, F. C. Krebs, *Sol. Energy Mater. Sol. Cells* **2010**, *94*, 2018.

[5] S. Wilken, J. Parisi, H. Borchert, *J. Phys. Chem. C* **2014**, *118*, 19672.

[6] D. A. Melnick, *J. Chem. Phys.* **1957**, *26*, 1136.

[7] S.-W. Fan, A. K. Srivastava, V. P. Dravid, *Appl. Phys. Lett.* **2009**, *95*, 142106.

[8] Y. Jiang, L. Sun, F. Jiang, C. Xie, L. Hu, X. Dong, F. Qin, T. Liu, L. Hu, X. Jiang, Y. Zhou, *Mater. Horiz* **2019**, *6*, 1438.

[9] S. Park, H. J. Son, *J. Mater. Chem. A* **2019**, *7*, 25830.

[10] A. Soultati, A. Verykios, S. Panagiotakis, K.-K. Armadorou, M. I. Haider, A. Kaltzoglou, C. Drivas, A. Fakharuddin, X. Bao, C. Yang, A. R. B. M. Yusoff, E. K. Evangelou, I. Petsalakis, S. Kennou, P. Falaras, K. Yannakopoulou, G. Pistolis, P. Argitis, M. Vasilopoulou, *ACS Appl. Mater. Interfaces* **2020**, *12*, 21961.

[11] M. Günther, D. Blätte, A. L. Oechsle, S. S. Rivas, A. A. Yousefi Amin, P. Müller-Buschbaum, T. Bein, T. Ameri, *ACS Appl. Mater. Interfaces* **2021**, *13*, 19072.

[12] H. Cha, J. Wu, A. Wadsworth, J. Nagitta, S. Limbu, S. Pont, Z. Li, J. Searle, M. F. Wyatt, D. Baran, J.-S. Kim, I. McCulloch, J. R. Durrant, *Adv. Mater.* **2017**, *29*, 1701156.

[13] N. Li, J. D. Perea, T. Kassar, M. Richter, T. Heumueller, G. J. Matt, Y. Hou, N. S. Güldal, H. Chen, S. Chen, S. Langner, M. Berlinghof, T. Unruh, C. J. Brabec, *Nat. Commun.* **2017**, *8*, 14541.

[14] X. Du, T. Heumueller, W. Gruber, A. Classen, T. Unruh, N. Li, C. J. Brabec, *Joule* **2019**, *3*, 215.

[15] X. Du, T. Heumueller, W. Gruber, O. Almora, A. Classen, J. Qu, F. He, T. Unruh, N. Li, C. J. Brabec, *Adv. Mater.* **2020**, *32*, 1908305.

[16] M. Chang, L. Meng, Y. Wang, X. Ke, Y.-Q.-Q. Yi, N. Zheng, W. Zheng, Z. Xie, M. Zhang, Y. Yi, H. Zhang, X. Wan, C. Li, Y. Chen, *Chem. Mater.* **2020**, *32*, 2593.

[17] M. O. Reese, S. A. Gevorgyan, M. Jørgensen, E. Bundgaard, S. R. Kurtz, D. S. Ginley, D. C. Olson, M. T. Lloyd, P. Morvillo, E. A. Katz, A. Elschner, O. Haillant, T. R. Currier, V. Shrotriya, M. Hermenau, M. Riede, K. R. Kirov, G. Trimmel, T. Rath, O. Inganäs, F. Zhang, M. Andersson, K. Tvingstedt, M. Lira-Cantu, D. Laird, C. McGuiness, S. (J.) Gowrisanker, M. Pannone, M. Xiao, J. Hauch, et al., *Sol. Energy Mater. Sol. Cells* **2011**, *95*, 1253.

[18] W. R. Mateker, M. D. McGehee, *Adv. Mater.* **2017**, 29.

[19] G. Ji, W. Zhao, J. Wei, L. Yan, Y. Han, Q. Luo, S. Yang, J. Hou, C.-Q. Ma, *J. Mater. Chem. A* **2019**, *7*, 212.

[20] L. Krishnan Jagadamma, M. T. Sajjad, V. Savikhin, M. F. Toney, I. D. W. Samuel, *J. Mater. Chem. A* **2017**, *5*, 14646.

[21] M. Chen, X. Wang, Y. Yu, Z. Pei, X. Bai, C. Sun, R. Huang, L. Wen, *Appl. Surf. Sci.* **2000**, *158*, 134.

[22] C. Lennon, R. B. Tapia, R. Kodama, Y. Chang, S. Sivananthan, M. Deshpande, *J. Electron. Mater.* **2009**, *38*, 1568.

[23] J. d. O. Primo, C. Bittencourt, S. Acosta, A. Sierra-Castillo, J.-F. Colomer, S. Jaerger, V. C. Teixeira, F. J. Anaissi, *Front. Chem.* **2020**, *8*, 571790.

[24] M. Takata, D. Tsubone, H. Yanagida, *J American Ceramic Soc.* **1976**, *59*, 4.

[25] M. Madel, F. Huber, R. Mueller, B. Amann, M. Dickel, Y. Xie, K. Thonke, *J. Appl. Phys.* **2017**, *121*, 124301.

[26] J. Lagowski, E. S. Sproles, H. C. Gatos, *J. Appl. Phys.* **1977**, *48*, 3566.

[27] Q. Liu, P. Mantilla-Perez, M. Montes Bajo, P. Romero-Gomez, J. Martorell, *ACS Appl. Mater. Interfaces* **2016**, *8*, 28750.

[28] Z. L. Wang, *J. Phys.: Condens. Matter* **2004**, *16*, R829.

[29] V. Bhatt, M. Kumar, J. Kim, H.-J. Chung, J.-H. Yun, *Ceram. Int.* **2019**, *45*, 8561.

[30] S. C. Abrahams, J. L. Bernstein, *Acta Crystallogr B Struct Sci* **1969**, *25*, 1233.

[31] N. Fairley, V. Fernandez, M. Richard-Plouet, C. Guillot-Deudon, J. Walton, E. Smith, D. Flahaut, M. Greiner, M. Biesinger, S. Tougaard, D. Morgan, J. Baltrusaitis, *Appl. Surf. Sci.* **2021**, *5*, 100112.